Available online at www.sciencedirect.com
SCIENCE DIRECT
Journal of Molecular Catalysis A: Chemical 239 (2005) 64–67
JOURNAL OF MOLECULAR CATALYSIS A: CHEMICAL
www.elsevier.com/locate/molcata

Influence of iron precursors on catalytic wet oxidation of H_2S to sulfur over Fe/MgO catalysts

Eun-Ku Lee [a,1], Kwang-Deog Jung [b,*], Oh-Shim Joo [b], Yong-Gun Shul [a]

[a] *Department of Chemical Engineering, Yonsei University, Seoul 120-749, Republic of Korea*
[b] *Eco-Nano Center, Korea Institute of Science and Technology, P.O. Box 131, Cheongryang, Seoul, Republic of Korea*

Received 31 August 2004; received in revised form 4 May 2005; accepted 22 May 2005
Available online 7 July 2005

Abstract

The Fe/MgO catalysts prepared from iron nitrate, iron chloride and iron sulfate were studied for catalytic wet oxidation of H_2S to sulfur. They were characterized using BET, XRD, H_2-TPR and TG/DSC techniques. Catalysts prepared from iron nitrate showed the highest H_2S removal ability among the prepared catalysts. Both the TPR and XPS analyses of the catalysts indicate that H_2S removal ability correlates with the dispersion of iron oxide in the Fe/MgO catalysts prepared from different iron precursors.

Keywords: Wet oxidation; H_2S; Iron precursor; Dispersion; TG/DSC

1. Introduction

The Claus process has been most commonly employed to remove H_2S from natural gas facilities or refinery plants. Claus plants generally convert 94–98% of sulfur compounds in the feed gas into elemental sulfur [1,2]. As the restrictions on sulfur emissions are annually strengthening worldwide, a number of tail gas clean-up processes have been developed to reduce sulfur emission to permissible levels [3]. The development of the new processes to deal with the Claus tail gas is based on the direct oxidation of remaining traces of H_2S by oxygen or H_2S absorption/recycling technologies [4–12].

Recently, iron supported on magnesia was suggested to be a good catalyst for catalytic wet oxidation of H_2S [13,14]. The high H_2S removal capacities of Fe/MgO could be explained by the finely dispersed iron oxide on the MgO support. These catalysts prepared by a dissolution–precipitation method resulted in high dispersion of Fe on the MgO support. The easy reduction of Fe^{3+} to Fe^{2+} in Fe/MgO by H_2S was attributed to the small particle size of Fe component in Fe/MgO. Thus, the importance of dispersing Fe particles well on the MgO support in H_2S wet oxidation should be emphasized. The amounts of paramagnetic Fe^{3+} cations on Fe/MgO were correlated with the H_2S removal abilities of Fe/MgO catalysts from Mössbauer experiments [14]. The active sites were attributed to these Fe^{3+} cations on Fe/MgO.

We previously reported that the Fe/MgO catalysts prepared by the suspension impregnation were more effective than those prepared by the incipient wetness impregnation for H_2S removal in catalytic wet oxidation [15]. In the case of the Fe/MgO catalysts prepared with iron nitrate, it was suggested that well dispersed Fe_2O_3 can be the active phase and that the formation of crystalline α-Fe_2O_3 should be avoided for H_2S oxidation.

In this study, we investigated the influence of the iron precursors on the structure and activity of Fe/MgO catalysts for catalytic wet oxidation of H_2S to elemental sulfur.

2. Experimental

Three Fe/MgO catalysts were prepared by a suspension impregnation method. Three kinds of salt precursors were

* Corresponding author.
E-mail addresses: ureka209@yonsei.ac.kr (E.-K. Lee), jkdcat@kist.re.kr (K.-D. Jung).
[1] Tel.: +82 2 21233554; fax: +82 2 3126401.

1381-1169/$ – see front matter © 2005 Elsevier B.V. All rights reserved.
doi:10.1016/j.molcata.2005.05.034

used: (i) iron nitrate ($Fe(NO_3)_3{\cdot}9H_2O$, Aldrich); (ii) iron sulfate ($Fe_2SO_4{\cdot}7H_2O$, Aldrich) and (iii) iron chloride ($FeCl_2$, Aldrich). MgO powder was dispersed into aqueous solutions of these iron precursors, respectively. The concentration of iron precursors in solution was controlled to obtain the desired Fe content on MgO. The suspension remained stirred for 4 h at room temperature in a rotary evaporator and then water was evaporated at 40 °C in a vacuum of 30 mbar. The obtained solid was kept in an oven at 110 °C overnight. Finally, it was calcined in air flow at 460 °C for 5 h. The dried samples with iron nitrate, iron sulfate and iron chloride are designated as Fe-N, Fe-S and Fe-Cl and the oxide samples after calcination at 460 °C are designated as Fe(N)/MgO, Fe(S)/MgO and Fe(Cl)/MgO, respectively.

Activity measurements were carried out using a stirred batch tank reactor. The catalyst samples (3.0 g, if not specified) were dispersed in the reactor charged with the distilled water (1.5 L, if not specified) and the reactant gases were supplied through a perforated rubber plate at the bottom of the reactor. H_2S concentrations from the reactor were measured with on-line G.C. with T.C.D. detector. A Porapak Q column (1/8 in. O.D. × 2 m) was used for separating the product gases.

The specific surface areas of the catalysts were obtained on an ASAP 2000 instrument by the BET method from the nitrogen adsorption isotherms at 77 K, taking a value of 0.164 nm^2 for the cross-section of nitrogen. The XRD patterns were collected with Rint 2000 (Rigaku Co.) using Cu Kα radiation (λ = 0.1542 nm). A thermogravimetric analyzer (TGA 2050, TA Instrument) and differential scanning calorimeter (DSC 2010, TA Instrument) were used for the investigation of thermal properties of the dried samples. XPS spectra were obtained using a Kratos XSAM 800 pci X-ray photoelectron spectrometer with Al Kα monochromatic X-ray (1487 eV) radiation. The charging effect of XPS spectra was carefully corrected with adventitious carbon at 284.6 eV as a reference.

3. Results and discussion

Fig. 1 shows the H_2S removal ability of Fe(N)/MgO, Fe(S)/MgO and Fe(Cl)/MgO catalysts with different iron loadings. Feed gases (H_2S: 5 mL/min, O_2: 100 mL/min) were introduced into the stirred slurry reactor with 1.5 L of distilled water and 3 g of catalyst. The H_2S removal ability was obtained by calculating the total amount of H_2S removed up to 50% of the H_2S removal efficiency. The maximized removal ability in H_2S oxidation was observed in the Fe concentration between 15 and 30 wt%. The removal ability of 15 wt% Fe/MgO depended on the iron precursor as follows: 3.75 gH_2S/g_{cat} for iron nitrate, 2.8 gH_2S/g_{cat} for iron sulfate and 2.4 gH_2S/g_{cat} for iron chloride, respectively. H_2S removal ability of Fe(N)/MgO catalyst is the highest in all of the ranges of iron loadings.

Table 1 shows the physical properties of 6 wt% Fe/MgO samples prepared from different precursors. BET surface

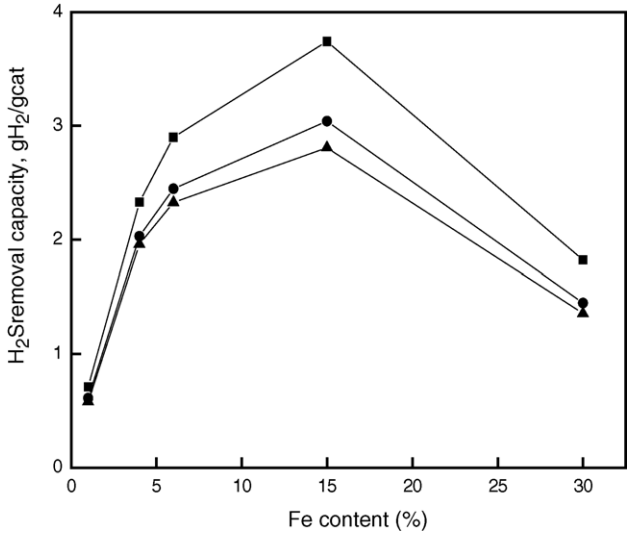

Fig. 1. H_2S removal abilities in H_2S catalytic wet oxidation over Fe(N)/MgO (■), Fe(S)/MgO (●) and Fe(Cl)/MgO (▲) and catalysts. H_2S flow rate: 5 mL/min, O_2 flow rate: 100 mL/min.

areas of Fe/MgO samples are in order of Fe(N)/MgO > Fe(S)/MgO > Fe(Cl)/MgO, which is correlated with H_2S removal ability. Therefore, the BET surface area can be responsible for the highest H_2S removal of the Fe(N)/MgO sample since Fe(N)/MgO samples have the highest BET surface area. The larger average pore diameter and pore volume of Fe(N)/MgO can be due to less sintering of Fe(N)/MgO as suggested by the high BET area and the high dispersion of the Fe component.

To understand the decomposition behavior of the precursor loaded on MgO during the calcinations, the TG–DSC profiles of Fe-N, Fe-S and Fe-Cl supported on MgO for preparing 6 wt% Fe/MgO were analyzed. Figs. 2 and 3 show the TG and DSC profiles of Fe-N, Fe-S and Fe-Cl samples, respectively. As shown in Fig. 2, two stages of weight loss can be observed on the TGA curve of the Fe-N sample. The first stage of weight loss of about 2–3% is observed between 0 and 300 °C and the second stage of weight loss of about 20% is observed above 300 °C. This corresponds to the two endothermic peaks on the DSC profiles (Fig. 3), demonstrating that the decomposition proceeded in two steps [16,17]:

Region I (<300 °C)

$$2Fe(NO_3)_3{\cdot}9H_2O \rightarrow 2Fe(NO_3)_3 + 9H_2O$$

Region II (>300 °C)

$$2Fe(NO_3)_3 + \tfrac{3}{2}O_2 \rightarrow \alpha\text{-}Fe_2O_3 + 6NO_3$$

Table 1
Physical properties of Fe/MgO prepared from different iron precursors

Sample	Iron precursor	S_{BET} (m^2/g)	Pore volume (cm^3/g)	Average pore diameter (Å)
Fe-N	Iron nitrate	32.2	0.18	223.4
Fe-S	Iron sulfate	25.7	0.07	109.2
Fe-C	Iron chloride	18.8	0.07	147.2

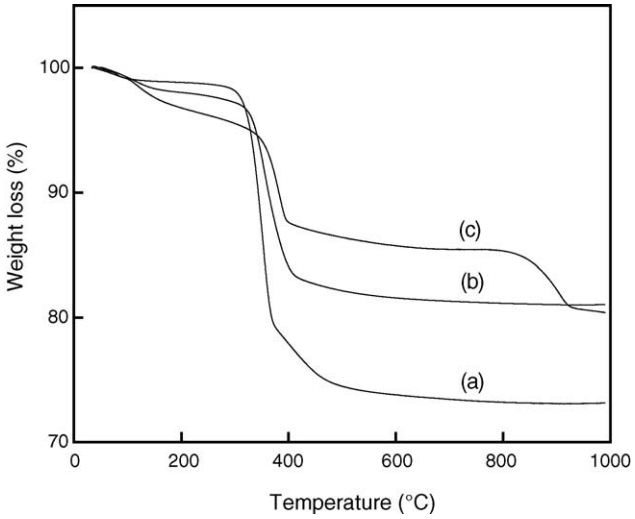

Fig. 2. TGA curves of Fe-N (a), Fe-Cl (b) and Fe-S (c) samples.

Three stages of weight loss are identified for the Fe-S sample. The first stage of weight loss can corresponds to the evolution of water, the second and the third stage of weight loss can be attributed to the evolution of gases. These reactions can occur [17]:

Region I (<300 °C)

$$FeSO_4 \cdot 7H_2O \rightarrow FeSO_4 \cdot H_2O + 6H_2O$$

Region II (300–480 °C)

$$6FeSO_4 \cdot H_2O + \tfrac{3}{2}O_2 \rightarrow \alpha\text{-}Fe_2O_3 + 2Fe_2(SO_4)_3 + 6H_2O$$

Region III (>480 °C)

$$2Fe_2(SO_4)_3 \rightarrow \alpha\text{-}Fe_2O_3 + 6SO_3$$

Two stages of weight losses of Fe-Cl sample are observed, which is similar to the TGA profile of the Fe-N sample. The first stage of weight loss can be primarily due to water loss. The second weight loss can be due to evolution of chloride in reduced (HCl) form. Temperature regions can be divided into two steps [17]:

Region I (<320 °C)

$$2FeCl_2 \cdot 4H_2O \rightarrow 2FeCl_2 \cdot H_2O + 6H_2O$$

Region II (>320 °C)

$$2FeCl_2 \cdot H_2O + \tfrac{1}{2}O_2 \rightarrow \alpha\text{-}Fe_2O_3 + 4HCl$$

Based on these results, the Fe(S)/MgO sample can partially contain the $Fe_2(SO_4)_3$ phase after calcined at 460 °C for 5 h, while Fe(N)/MgO and Fe(Cl)/MgO samples cannot have each precursor phase. The optimum calcinations temperature of 460 °C was for preparing well dispersed Fe/MgO catalyst: the higher calcination temperature than 460 °C resulted in the lower H_2S removal ability of Fe/MgO catalyst due to the agglomeration of α-Fe_2O_3.

Fig. 4 shows XRD patterns for the 6 wt% Fe/MgO catalysts after calcination at 460 °C. The sharp diffraction peaks at $2\theta = 36.9$, 42.9, 62.3, 74.6 and 78.6° are ascribed to the MgO support (JCPDS 4-829). All of Fe/MgO catalysts show the peaks attributable to MgO and no evidence for Fe_2O_3, indicating that well dispersed Fe particles can be present on Fe/MgO catalysts, regardless of the kind of Fe precursor.

Fig. 5 shows the TPR profiles of 6 wt% Fe/MgO catalysts prepared from different iron precursors. TPR patterns of these catalysts exhibit quite different peaks. Fe(N)/MgO sample shows the first peak at 570 °C, whereas for Fe(S)/MgO and Fe(Cl)/MgO samples the first peak appears at 650 and 680 °C, respectively. The first TPR peak corresponds to the reduction of the highly dispersed Fe_2O_3 species, which are not detected by the XRD. The second peak can be ascribed to the reduction of $Mg_2Fe_2O_4$ species, which was previously

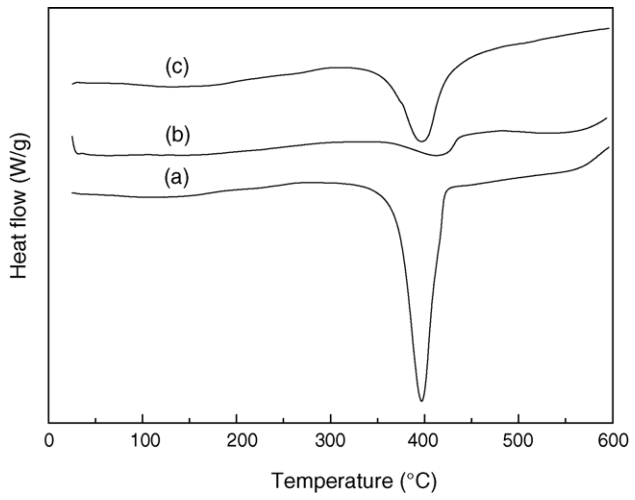

Fig. 3. DSC curves of Fe-N (a), Fe-S (b) and Fe-Cl (c) samples.

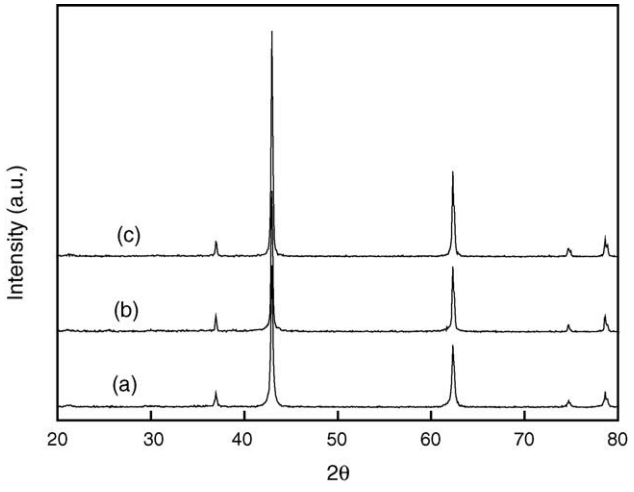

Fig. 4. X-ray diffraction patterns of Fe(N)/MgO (a), Fe(S)/MgO (b) and Fe(Cl)/MgO (c) catalysts.

Table 2
XPS binding energies and surface atomic ratios of Fe/MgO catalysts determined by XPS peak areas

Fe precursor	Binding energy (eV)		Atomic ratio			
	Fe 3/2p	Mg 2p	Fe/Mg × 10^{-2}	NO^{3-}/Fe × 10^{-3}	SO_4^{2-}/Fe × 10^{-3}	Cl^-/Fe × 10^{-3}
Nitrate	710.9 ± 0.1	49.8 ± 0.1	4.63	–	–	–
Sulfate	710.8 ± 0.2	49.6 ± 0.3	3.75	–	1.2	–
Chloride	710.9 ± 0.2	49.7 ± 0.1	2.49	–	–	–

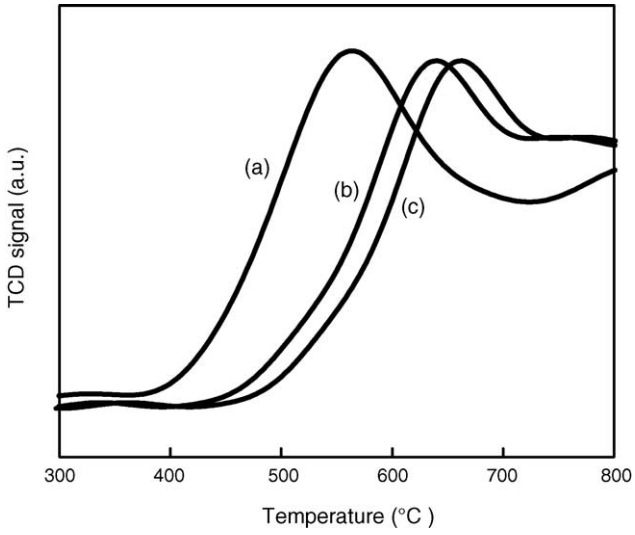

Fig. 5. TPR profiles of Fe(N)/MgO (a), Fe(S)/MgO (b) and Fe(Cl)/MgO (c) catalysts.

confirmed by Mössbauer spectroscopy [14]. These results can be related to the Fe_2O_3 particle size in Fe/MgO catalysts, indicating that Fe(N)/MgO shows the highest iron dispersion.

The binding energies (BE) of some characteristic core levels of Fe and Mg in the samples and atomic surface ratios are shown in Table 2 [18,19]. The presence of sulfate ion on the Fe(S)/MgO sample surface was detected by the binding energy at around 168.7 eV [20], indicating that the catalyst prepared from iron sulfate has sulfur species on the catalyst surface. In all cases, the binding energies are essentially constant for the catalyst, regardless of the kind of the salt precursor [21]. It is concluded that the Fe/MgO samples are all in a similar valence state, indicating no electronic effect of Fe precursor regardless of precursors. The peak intensity ratios of Fe/MgO were calculated using atomic-sensitive factors. The atomic ratio of Fe to Mg on the surface of catalysts increase in the order: chloride < sulfate < nitrate samples. It indicates that the Fe sites are lower in density on Fe-S and Fe-C catalysts. So, it is concluded that the difference in precursor affected the number of active sites on the surface, resulting in activity differences of H_2S wet oxidation.

4. Conclusions

The effect of metal precursor on H_2S wet oxidation was found over Fe/MgO catalysts. The catalysts show quite different H_2S removal abilities. The Fe(N)/MgO catalyst shows the highest H_2S removal ability in H_2S wet oxidation because there are higher active sites on the catalyst, as estimated by XPS studies. The TPR study suggests that the iron precursors have an important effect on the dispersion of iron oxide and on the catalytic behaviors of the final catalysts. TGA/DSC analysis indicates that Fe-related phases are present as α-Fe_2O_3 in the Fe-N and Fe-C catalysts while α-Fe_2O_3 and $Fe_2(SO_4)_3$ phases can coexist in the Fe(S)/MgO catalyst.

References

[1] J.W. Estep, G.T. McBride, J.R. West, Advances in Petroleum Chemistry and Refining, vol. 6, Interscience, New York, 1962, p. 315.
[2] B.G. Goar, Oil Gas J. 25 (1975) 96.
[3] Anon., Sulfur 20 (1995) 236.
[4] N. Keller, C.P. Huu, M.J. Ledoux, Appl. Catal. 217 (2001) 205.
[5] G.E. Vrieland, C.B. Murchison, Appl. Catal. 134 (1996) 101.
[6] J. Ogonowski, Chem. Stosow. 33 (1989) 281.
[7] J. Ogonowski, Nafta-Gas 49 (1993) 269.
[8] V.P. Luk'yanenko, D.N. Tmenov, V.S. Solodkaya, Neftepererab. Neftekhim. (Kiev) 46 (1994) 14.
[9] L.E. Cadus, M.C. Abello, M.F. Gomez, J.B. Rivarla, Ind. Eng. Chem. Res. 35 (1996) 14.
[10] F.C. Meunier, A. Yasmeen, J.R.H. Ross, Catal. Today 37 (1997).
[11] K.H. Lee, Y.S. Yoon, W. Ueda, Y. Moro-Oka, Catal. Lett. 46 (1997) 267.
[12] J. Shimada, T. Sato, Y. Yoshimura, J. Hiraishi, A. Nishijima, J. Catal. 110 (1988) 275.
[13] K.D. Jung, O.S. Joo, S.H. Cho, S.H. Han, Appl. Catal. 240 (2001) 213.
[14] K.D. Jung, O.S. Joo, C.S. Kim, Catal. Lett. 84 (2002) 53.
[15] E.K. Lee, K.D. Jung, O.S. Joo, Y.G. Shul, Bull. Kor. Chem. Soc. 26 (2005) 281.
[16] J. Shen, B. Guang, M. Tu, Y. Chen, Catal. Today 30 (1996) 77.
[17] R.M. Cornell, U. Schwertmann, The Iron Oxides, Wiley-VCH, 2003, p. 526.
[18] P.C.J. Graat, M.A.J. Somers, Appl. Surf. Sci. 100 (1996) 36.
[19] G.A. Bukhtiyarova, V.I. Bukhtiyarov, N.S. Sakaeva, V.V. Kaichev, B.P. Zolotovskii, J. Mol. Catal. 158 (2000) 251.
[20] A.C. Oliveira, J.L.G. Fierro, A. Valentini, P.S.S. Nobre, M.D.C. Rangel, Catal. Today 85 (2003) 49.
[21] W.-J. Shen, Y. Ichihashi, H. Ando, M. Okumura, M. Haruta, Y. Matsumura, Appl. Catal. 217 (2001) 165.